Dyes and Pigments 92 (2012) 1083–1090

Contents lists available at SciVerse ScienceDirect

Dyes and Pigments

journal homepage: www.elsevier.com/locate/dyepig

A new rhodamine-based single molecule multianalyte (Cu^{2+}, Hg^{2+}) sensor and its application in the biological system

Lina Wang [a], JieXi Yan [b], Wenwu Qin [a], Weisheng Liu [a,*], Rui Wang [b]

[a] Key Laboratory of Nonferrous Metals Chemistry and Resources Utilization of Gansu Province and State Key Laboratory of Applied Organic Chemistry, College of Chemistry and Chemical Engineering, Lanzhou University, Lanzhou 730000, PR China
[b] Key Laboratory of Preclinical Study for New Drugs of Gansu Province, School of Basic Medical Sciences, School of Life Sciences, and State Key Laboratory of Applied Organic Chemistry, Lanzhou University, Lanzhou 730000, PR China

ARTICLE INFO

Article history:
Received 23 February 2011
Received in revised form
21 July 2011
Accepted 24 July 2011
Available online 23 August 2011

Keywords:
Multianalyte sensor
Cu^{2+}
Hg^{2+}
Fluorescence
Imaging
Living cells

ABSTRACT

A new single molecule multianalyte sensor, vanillic aldehyde rhodamine 6G hydrazone has been designed for the selective detection of Cu^{2+} and Hg^{2+} ions. UV/Vis spectroscopy indicates that the sensor is a good chromogenic chemosensor for Cu^{2+} in 1:99 (v/v) ethanol–water media. Whereas, other ions, such as Li^{+}, Na^{+}, Mg^{2+}, K^{+}, Ca^{2+}, Cr^{3+}, Mn^{2+}, Fe^{3+}, Co^{2+}, Ni^{2+}, Zn^{2+}, Ag^{+}, Cd^{2+}, Ba^{2+}, Hg^{2+} and Pb^{2+} failed to generate a distinct response. Fluorescence spectral data reveals that the sensor is an excellent fluorescent chemosensor for Hg^{2+} in aqueous ethanol solution and with no fluorescent response toward other ions. The spectroscopic behavior of the sensor in living cells indicated that it can be used for the detection of Cu^{2+} and Hg^{2+} in environmental and biological systems. Mechanisms for the high selectivity of the sensor to Cu^{2+} and Hg^{2+} are discussed.

1. Introduction

The design of chemosensors for the detection of heavy- and transition-metal (HTM) ions, such as copper and mercury, is particularly attractive because these ions play important roles in living systems and have an extremely toxic impact on the environment [1]. Copper plays a critical role as a catalytic cofactor for a variety of metalloenzymes, however, copper exhibits toxicity under overload conditions, causing neurodegenerative disease [2]. Mercury induces a great threat because both elemental and ionic mercury can be converted by bacteria in the environment to the highly toxic methyl mercury, which subsequently bioaccumulates through the food chain [3], leading to many health problems in the brain, kidney, and central nervous system [4]. Thus, much effort has been devoted to the development of chemosensors for Cu^{2+} and Hg^{2+}. A number of Cu^{2+} and Hg^{2+} sensors have been reported in recent years [5]. Unfortunately, some of the Cu^{2+} sensors have disadvantages such as poor water-solubility or UV light excitation. Most of the reported chemodosimeters for Hg^{2+} are based on thiophilicity [6]. It is hard to avoid interference from mercapto-chemicals in an organism and sulfur-rich environments in the detection of Hg^{2+}. Overcoming these disadvantages in the design of excellent indicators for Cu^{2+} and Hg^{2+} is a challenging task.

The rhodamine framework is an ideal template to use in constructing chelation-enhanced fluorescence (CHEF) OFF–ON fluorescent chemosensors for metal ions due to its particular structural properties. Without cations, these rhodamine-based chemosensors exist in a spirocyclic form which is colorless and non-fluorescent. The addition of a specific metal ion leads to spirocycle opening via coordination or irreversible chemical reaction [7], resulting in the appearance of a pink color or orange fluorescence. In addition, rhodamine-based compounds are ideal candidates for fluorescent sensors because of their good photophysical properties, such as absorption and emission wavelengths elongated to the visible region, high fluorescence quantum yield, and large absorption coefficient [8]. In our previous work, we have reported an excellent rhodamine-based fluorescent sensor for Fe^{3+} and Cr^{3+} in aqueous solution [9]. Herein, we report a rhodamine-based spirolactam derivative (**L**) as a chemosensor for Cu^{2+} and Hg^{2+} by ultraviolet–visible or fluorescence spectrophotometry. This dual signaling is of significance because receptors that are able to display sensing abilities to different cations when using different signaling channels are very rare [10].

* Corresponding author. Tel.: +86 931 8915151; fax: +86 931 8912582.
E-mail address: liuws@lzu.edu.cn (W. Liu).

0143-7208/$ – see front matter © 2011 Published by Elsevier Ltd.
doi:10.1016/j.dyepig.2011.07.010

2. Experimental section

2.1. Instruments and reagents

All the materials for the syntheses were purchased from commercial suppliers and used without further purification. All of the solvents used were of analytical reagent grade. Water was deionized. The solutions of the metal ions were prepared from their perchlorate salts, except for K^+ which was available as KNO_3. HEPES buffer solutions (1×10^{-2} mol L^{-1}, pH = 7.0) were prepared in water.

^1H and ^{13}C NMR spectra were taken on a Varian Mercury-300 spectrometer with tetramethylsilane (TMS, 0.00 ppm) as an internal standard and $CDCl_3$ as solvent. Chemical shift multiplicities are reported as s = singlet, d = doublet, t = triplet, q = quartet and m = multiplet. MS spectra were determined on a Bruker Daltonics Esquire 6000 spectrometer. Absorption spectra were determined on a Varian UV-Cary100 spectrophotometer using quartz cells of 1.0×10^{-2} m path length. Fluorescence spectra measurements were performed on a Hitachi F-4500 spectrofluorimeter and a Shimadzu RF-540 spectrofluorophotometer equipped with quartz cuvettes of 10 mm path length with a xenon lamp as the excitation source. An excitation and emission slit of 5.0 nm or 2.5 nm were used for the measurements in the solid state. Quantum yields were determined by an absolute method using an integrating sphere based upon that originally developed by de Mello et al. [11], using an FLS920 supplied by Edinburgh Instrument. All pH measurements were made with a pH-10C digital pH meter. All spectra were recorded at room temperature except for fluorescence microscope images. The fluorescence microscope experiment was carried out with a Nikon TE2000-5.

2.2. Cell incubation and imaging

Images of human bladder cancer cell line EJ: Human bladder cancer cell line EJ were obtained from Laboratory Center for Medical Science of Lanzhou University. Cells were cultured in RPMI 1640 (Gibco, NY) supplemented with 10% Fetal Bovine Serum (FBS, rongye Bio-tech, China) and penicillin (1×10^5 U L^{-1})/streptomycin (1×10^{-4} kg L^{-1}) in an atmosphere of 5% CO_2 at 37 °C. One day before imaging, cells were seeded in 96-well flat-bottomed plates. Immediately before the experiments, incubating cells with the probe **L** (2.5×10^{-5} mol L^{-1}) and supplementing cells with 2.5×10^{-5} mol L^{-1} $Cu(ClO_4)_2$ or $Hg(ClO_4)_2$ in ethanol–PBS (1:4, v/v, PBS: phosphate-buffered saline) at 37 °C under 5% CO_2 for 0.5 h. The cells were washed with PBS three times and then imaged. The fluorescence imaging of intracellular was observed under a Nikon Eclipse TE2000-5 inverted fluorescence microscopy with 20× objective or 40× objective lens (excited with green light). The EJ cells only incubated with **L** (2.5×10^{-5} mol L^{-1}) for 0.5 h at 37 °C under 5% CO_2 was as a control.

Images of human leukemia K562 cells: human leukemia K562 cells were obtained from Laboratory Center for Medical Science of Lanzhou University. Cells were cultured in RPMI 1640 (Gibco, NY) supplemented with 10% Fetal Bovine Serum (FBS, rongye Bio-tech, China) and penicillin (1×10^5 U L^{-1})/streptomycin (1×10^{-4} kg L^{-1}) in an atmosphere of 5% CO_2 at 37 °C. One day before imaging, cells were harvested by centrifugation and resuspended in PBS buffer. Immediately before the experiments, cells were incubated with the probe **L** (2.5×10^{-5} mol L^{-1}) at 37 °C under 5% CO_2, and they were exposed to 2.5×10^{-5} mol L^{-1} $Cu(ClO_4)_2$ or $Hg(ClO_4)_2$ in ethanol–PBS (1:4, v/v) for 0.5 h. The cells were washed with PBS three times. And then they were passed into a 96-well plate and imaged. The fluorescence imaging of intracellular was observed under a Nikon Eclipse TE2000-5 inverted fluorescence microscopy with a 40× objective lens (excited with green light). The K562 cells only incubated with **L** (2.5×10^{-5} mol L^{-1}) for 0.5 h at 37 °C under 5% CO_2 was as a control.

2.3. Preparation of rhodamine sensor (*L*)

Compound **L** was synthesized from rhodamine 6G by a simple two-step reaction as depicted in Scheme 1. Rhodamine 6G hydrazone is prepared according to the literature method [12].

Rhodamine 6G hydrazide (1.0 mmol, 0.428 g) and vanillic aldehyde (1.0 mmol, 0.152 g) were mixed in boiling ethanol then the mixture was refluxed in an air bath for 6 h. After that, the solution was cooled and allowed to stand at room temperature overnight. The precipitate which appeared next day was filtered and washed 3 times with 10 mL cold ethanol. After drying under reduced pressure, the reaction afforded 0.390 g (0.69 mmol) **L** (69%) as white solid. ^1H NMR (300 MHz, $CDCl_3$): δ 11.96 (s, 1H), 9.11 (s, 1H), 8.0–7.97 (*t*, 1H, *J* = 3.9 Hz), 7.50–7.47 (*t*, 2H, *J* = 2.7 Hz), 7.08–7.06 (*t*, 1H, *J* = 4.1 Hz), 6.81–6.71 (m, 3H), 6.38 (s, 2H), 6.30 (s, 2H), 3.82 (s, 3H), 3.47 (s, 2H), 3.22–3.15 (m, 4H), 1.89 (s, 6H), 1.32–1.27 (*t*, 6H, *J* = 6.9 Hz); ^{13}C NMR (75 MHz, $CDCl_3$) δ 164.55, 152.63, 151.73, 151.50, 148.15, 148.02, 147.53, 133.55, 128.94, 128.36, 127.56, 123.91, 123.26, 123.17, 118.45, 117.95, 113.04, 105.25, 96.83, 66.21, 55.92, 38.24, 16.71, 14.68 ppm; ESI-MS: *m/z* obsd 563.3 ($[M + H]^+$ calcd 563.3 for $C_{34}H_{34}N_4O_4$).

3. Results and discussion

Solutions of **L** in aqueous or organic media are colorless and non-fluorescent, indicating that the spirolactam form of **L** predominates. The characteristic peak near 66 ppm in the ^{13}C NMR spectra of **L** also supports this conclusion [13]. The significant change in visible absorption spectra of **L** after the addition of Cu^{2+} makes **L** a selective visual chemosensor for rapid and selective detection of Cu^{2+}. Interestingly, **L** is an excellent fluorescent chemosensor for Hg^{2+} in biosystems and abiotic systems.

Fig. 1 shows the absorption spectra of **L** in the presence of various metal ions in 1:99 ethanol/H_2O (v/v, pH 7.0) solution. The absorption spectra of **L** alone (2×10^{-5} mol L^{-1}) exhibited no band above 500 nm, which indicated **L** was in the spirolactam form. Upon the addition of Cu^{2+} ion, a strong absorption band centered at 530 nm appeared, corresponding to a clear color change from colorless to pink (Fig. S1). A slight increase at 530 nm after the addition of Hg^{2+} and Fe^{3+} was also observed at the same concentration. We conclude that Fe^{3+} and Hg^{2+} have lower binding affinity

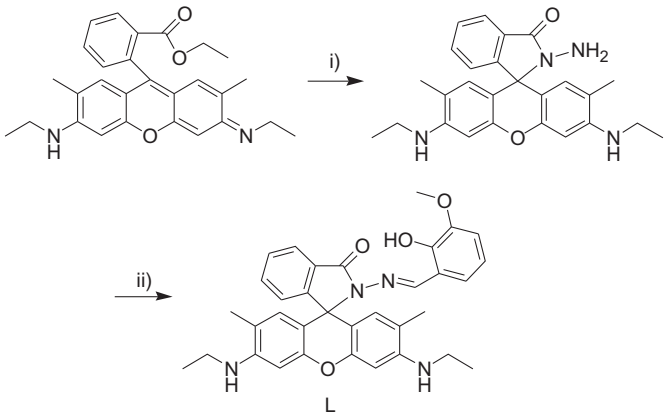

Scheme 1. Synthetic route of target sensors: i) hydrazine hydrate, ethanol, reflux, 2 h, 91%; ii) vanillic aldehyde, ethanol, reflux, 8 h, 69%.

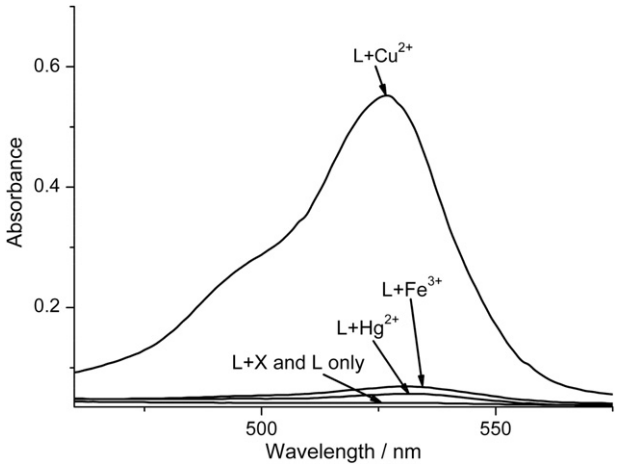

Fig. 1. Absorption spectra of **L** (2×10^{-5} mol L^{-1}) in 1:99 ethanol/H_2O (v/v, pH 7.0) in the presence of different cations (5 equiv, respectively).

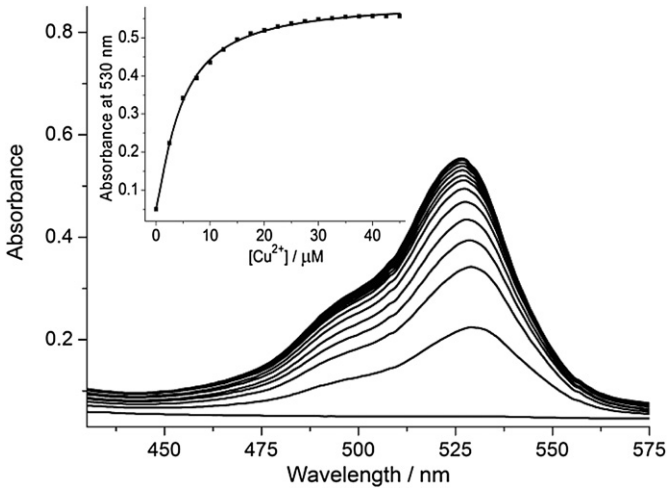

Fig. 3. Absorption spectra of **L** (2×10^{-5} mol L^{-1}) upon addition of increasing amounts of Cu^{2+} in 1:99 ethanol/H_2O (v/v, pH 7.0). Inset: absorbance at 530 nm as a function of Cu^{2+} concentration, indicating a 1:1 metal–ligand ratio.

to **L** compared with Cu^{2+} in aqueous media. **L** exhibits no change in absorbance at 530 nm after addition of 5.0 equiv of other metal ions in 1:99 ethanol/H_2O (v/v) solution. Therefore, **L** can serve as a highly selective visual chemosensor for Cu^{2+}. An important feature of the sensor is its high selectivity toward the analyte over other competitive species. The addition of Cu^{2+} ion still resulted in large absorption changes even in the presence of miscellaneous competitive cations (Fig. 2). This indicates that the selectivity of **L** for the Cu^{2+} over other competitive cations in the water medium is remarkably high. The nice nonlinear fitting of the absorbance against Cu^{2+} concentration (Fig. 3) indicated a 1:1 binding stoichiometry between **L** and Cu^{2+}. The ESI-mass spectra of **L**–Cu^{2+} also showed a 1:1 stoichiometry. The unique peak at $m/z = 625.4$ (calcd = 625.2) corresponding to $[CuL]^+$ was clearly observed when Cu^{2+} was added to **L** (Fig. S5). **L** without Cu^{2+} exhibited peak only at $m/z = 563.3$ (calcd = 563.3) which corresponded to $[L + H]^+$. Job's plots also suggested that a 1:1 stoichiometry is the most likely binding mode between **L** and Cu^{2+} (Fig. 4) [14]. To achieve this 1:1 stoichiometry, carbonyl O, imino N, and phenol O atoms of **L** are the most likely binding sites for Cu^{2+}. Scheme 3 displays the proposed structure of **L**–Cu^{2+}.

For practical applicability, the optimal pH condition of chemodosimeter **L** was evaluated. Fig. 5 shows that for free **L**, the absorbance intensity is strong when pH < 4. It is due to that the ring opening of rhodamine occurred at acid conditions (pH < 4) for the strong protonation. No obvious absorbance was observed when pH > 4. However, the absorbance intensity has significant enhancement after the addition of Cu^{2+} ion between pH 4 and 10. Fig. 5 shows that **L** can detect Cu^{2+} ion with a wide pH span (3–12). This is because of the **L**–Cu^{2+} complex formed with the addition of Cu^{2+} ion in this pH region. **L** is colorless without Cu^{2+} ion since the spirolactam form of **L** predominates.

The change of fluorescence spectrum of **L** in the presence of various metal ions was investigated in ethanol. The fluorescence emission band of **L** near 550 nm is very weak. Significant enhancement in fluorescence intensity was created upon addition of Hg^{2+} or Cr^{3+} (Fig. 6), and the emission quantum yields (Φ) were 0.335 and 0.445, respectively. However, fluorescence produced by

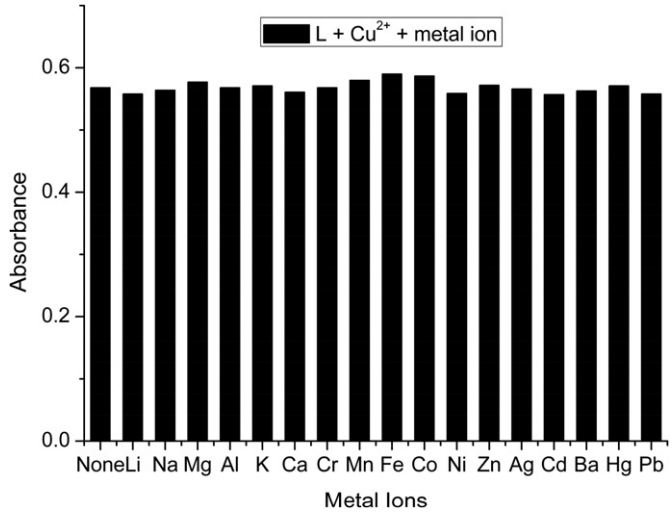

Fig. 2. Selectivity of **L** (2×10^{-5} mol L^{-1}) for Cu^{2+} (1×10^{-4} mol L^{-1}) over other cations. The bars indicate the absorbance change that occurs immediately following the addition of interfering ions (1.0 equiv. of the Cu^{2+} ions) to the 1:99 ethanol/H_2O (v/v, pH 7.0) solution containing **L** and Cu^{2+} ions, the absorption wavelength is 530 nm.

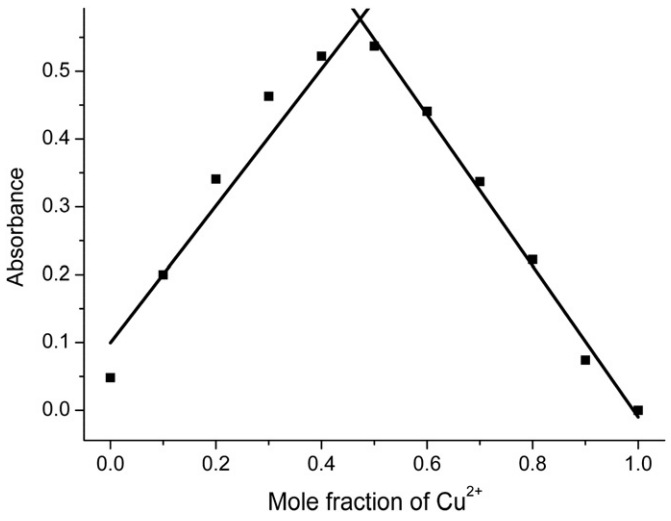

Fig. 4. Plots according to the method for continuous variations, indicating the 1:1 stoichiometry of the **L**–Cu^{2+} complex. The total concentration of **L** and Cu^{2+} ion is 4×10^{-5} mol L^{-1}.

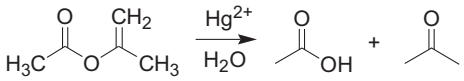

Scheme 2. Mercury-promoted hydrolysis of isopropenyl acetate.

the addition of Cr^{3+} disappeared after the addition of a small amount of water to the ethanol. No such obvious change was found in the fluorescence that depended on the appearance of Hg^{2+} ion. The change of fluorescence intensity in different ratios of water-ethanol mixtures upon the addition of Hg^{2+} or Cr^{3+} was studied (Fig. 7). Fig. 7 shows that the fluorescence intensity of **L**–Hg^{2+} declines slowly with the addition of water content. In contrast, the fluorescence upon the chelation of **L** and Cr^{3+} quenched quickly after the addition of water to ethanol. As we know, the coordination ability of Cr^{3+} with water is very strong. The rapid quenching of the **L**–Cr^{3+} complex may be caused by hydrolysis upon the addition of water. The hydrolysis between H_2O and Cr^{3+} result in the formation of $Cr(OH)_3$, which can inhibit the formation of complex between **L** and Cr^{3+}. Thus, **L** has good selectivity to Hg^{2+} ion in ethanol–water mixtures. The responses of other ions, such as Li^+, Na^+, K^+, Ca^{2+}, Mn^{2+}, Fe^{3+}, Co^{2+}, Ni^{2+}, Cu^{2+}, Zn^{2+}, Ag^+, Cd^{2+}, Ba^{2+} and Pb^{2+}, to **L** in fluorescence spectra in ethanol were also investigated. Most of these ions gave no visible change except for Zn^{2+} and Fe^{3+}, which caused faint increases compared to Cr^{3+} and Hg^{2+}. The open ring form of **L** created by the binding of Cu^{2+} has no fluorescence, which is ascribed to the quenching of the fluorescence by Cu^{2+}, based on the well-known paramagnetic effect of the d^9 Cu^{2+} system [15].

Fig. 8 illustrates the fluorescence emission changes of **L** in 50% ethanol–water at pH 7.0 upon the addition of various metal ions. Minimal fluorescence near 555 nm was observed in the fluorescence spectrum of **L**. The fluorescence intensity of a solution of **L** containing Hg^{2+} ion increases largely, and the emission quantum yield was 0.298. The response of the fluorescence spectra upon adding other ions to **L** was investigated. A tiny increase was detected when Fe^{3+} or Cr^{3+} was added to a solution of **L**. Other ions gave no distinct response in ethanol–water mixtures. Fig. 9 shows the fluorescence response of **L** to Hg^{2+} in the presence of miscellaneous competitive ions in 50% ethanol–water solution. A background of most selected coexistent metal ions does not interfere with the sensing of **L** for Hg^{2+}. The existence of Cu^{2+} can interfere with Hg^{2+} detection. But Hg^{2+} also induced large enhancement of

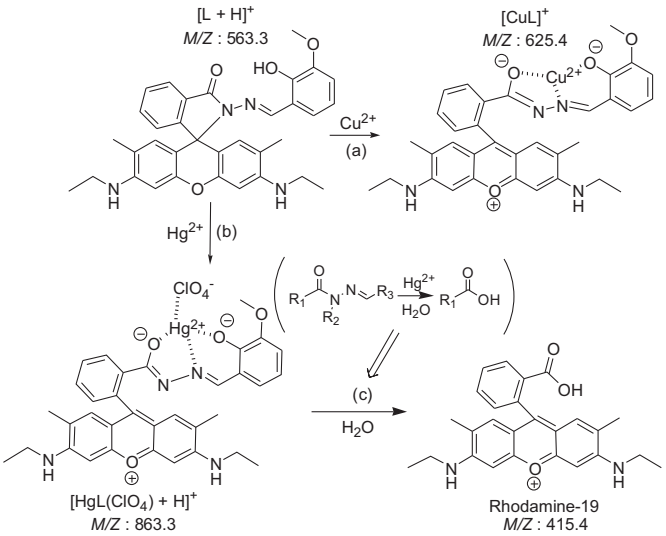

Scheme 3. Proposed binding stoichiometry of **L** with metal ions.

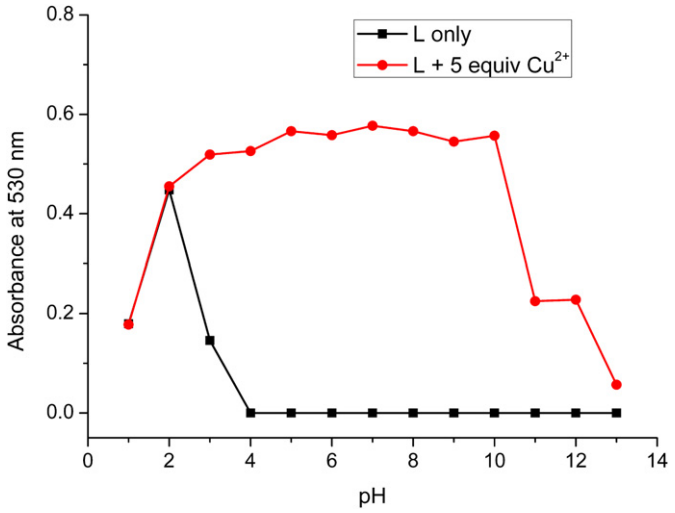

Fig. 5. Absorption intensity (530 nm) of free **L** (2×10^{-5} mol L^{-1}) and **L** + 5 equiv of Cu^{2+} ion in 1:99 ethanol/H_2O (v/v) with different pH conditions.

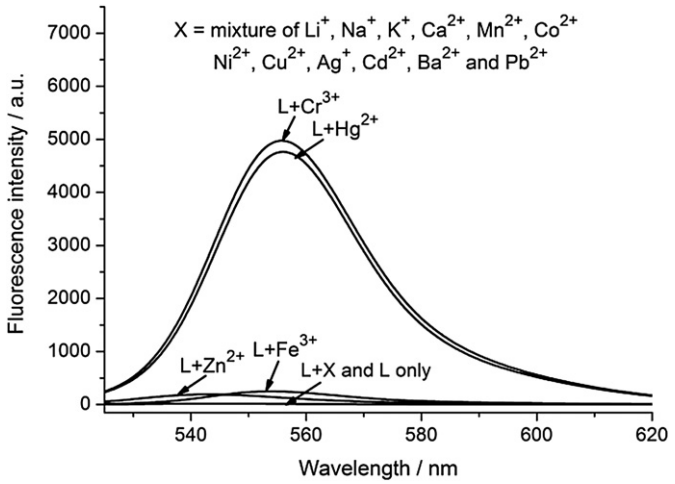

Fig. 6. Fluorescence spectra of **L** (2×10^{-5} mol L^{-1}) in the presence of different metal ions (5 equiv, respectively) in ethanol. The excitation wavelength is 515 nm.

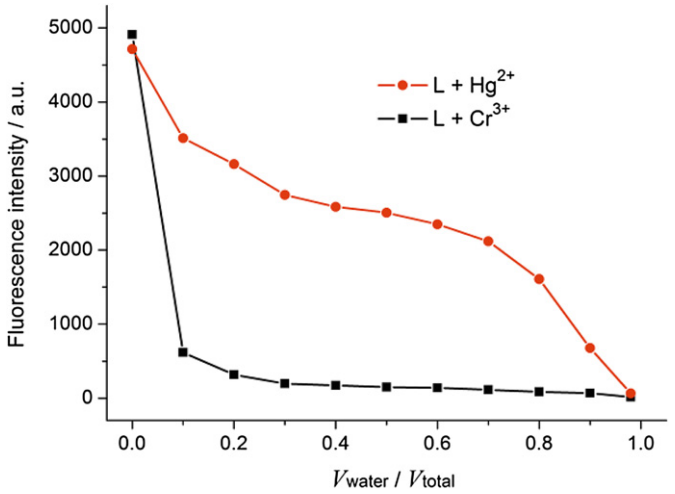

Fig. 7. Fluorescence spectrum of **L** (2×10^{-5} mol L^{-1}) upon the addition of Hg^{2+} or Cr^{3+} (1×10^{-4} mol L^{-1}) in different ratios of water–ethanol mixtures (total: water + ethanol. $\lambda_{ex} = 515$ nm).

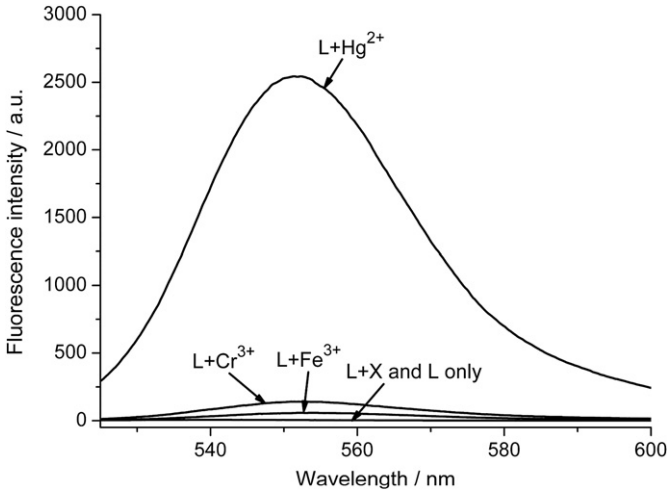

Fig. 8. Fluorescence spectra of **L** (2×10^{-5} mol L^{-1}) in 50% ethanol–water (pH 7.0) in the presence of the Hg^{2+} ion and miscellaneous cations (5 equiv, respectively. $\lambda_{ex} = 515$ nm). Each spectrum was acquired 10 min after Hg^{2+} addition.

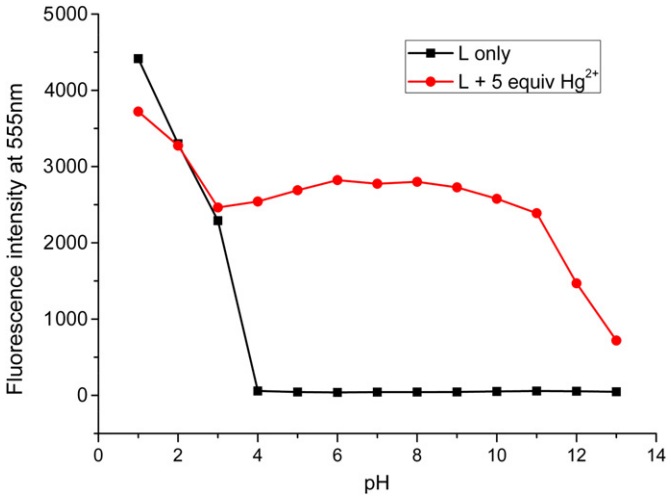

Fig. 10. Fluorescence intensity (555 nm) of free **L** (2×10^{-5} mol L^{-1}) and **L** + 5 equiv of Hg^{2+} ion in 1:1 ethanol/H_2O (v/v) with different pH conditions.

fluorescence intensity even in the presence of Cu^{2+} ions. The results indicate that **L** is a good fluorescence probe for Hg^{2+} in ethanol–water medium.

The effects of pH on the sensor **L** was evaluated. Fluorescence pH titrations of the sensor were carried out in 50% aqueous ethanol (v/v) solution. Fig. 10 shows that for free **L**, the fluorescence intensity is strong at pH < 4. It is due to that the ring opening of rhodamine took place for the strong protonation. No obvious fluorescence was observed when pH > 4. However, the fluorescence intensity increased largely after the addition of Hg^{2+} ion between pH 4 and 11. Fig. 10 shows that **L** can detect Hg^{2+} ion with a wide pH span. This is because of Hg^{2+}-promoted ring opening and hydrolysis. **L** is colorless without Hg^{2+} ion since the spirolactam form of **L** predominates.

The ESI-mass spectrum analysis of **L**–Hg^{2+} was performed to explore the mechanism. The peaks at $m/z = 763.4$ (calcd = 763.2) and $m/z = 863.3$ (calcd = 863.2) corresponding to $[HgL]^+$ and $[HgL(ClO_4) + H]^+$ were observed, respectively, in organic solvent

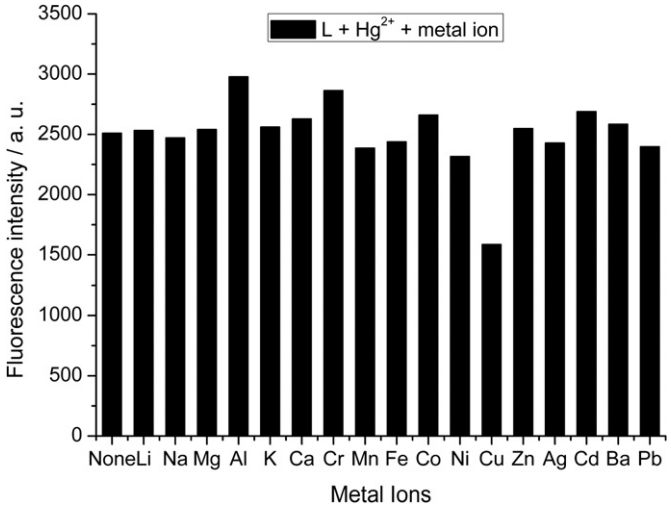

Fig. 9. Selectivity of **L** (2×10^{-5} mol L^{-1}) for Hg^{2+} (1×10^{-4} mol L^{-1}) over other cations. The bars indicate the fluorescence change that occurs immediately following the addition of interfering ions (1.0 equiv. of the Hg^{2+} ions) to the 1:1 ethanol/H_2O (v/v, pH 7.0) solution containing **L** and Hg^{2+} ions, the emission wavelength is 555 nm.

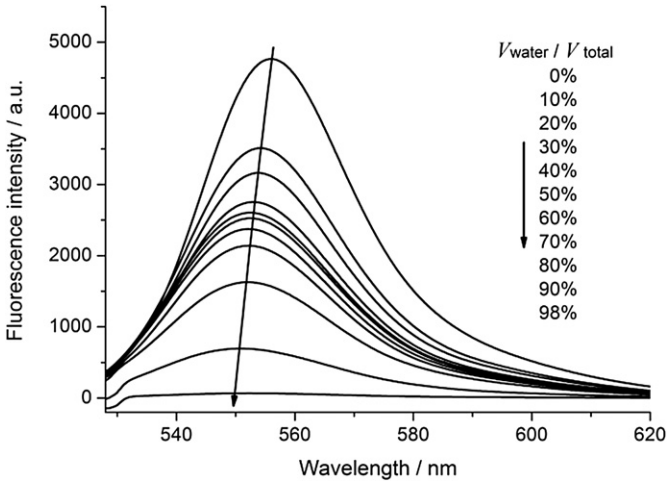

Fig. 11. Fluorescence spectra of **L** (2×10^{-5} mol L^{-1}) upon addition of Hg^{2+} (1×10^{-4} mol L^{-1}) in ethanol containing different concentrations of water (total: water + ethanol. $\lambda_{ex} = 515$ nm). Each spectrum was acquired 10 min after Hg^{2+} addition.

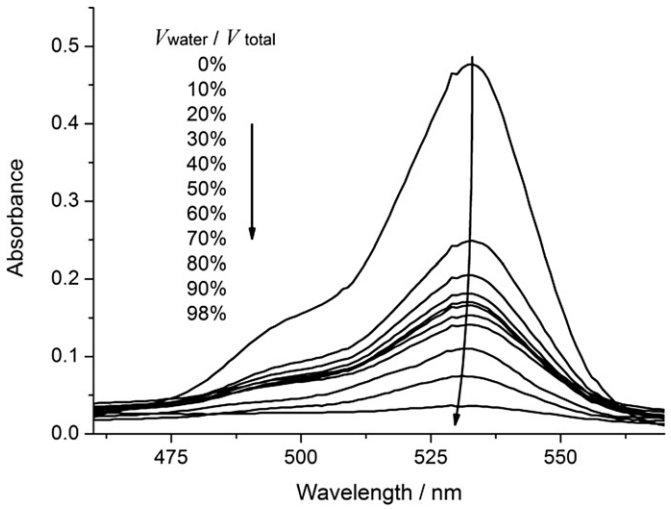

Fig. 12. Absorption spectra of **L** (2×10^{-5} mol L^{-1}) upon addition of Hg^{2+} (1×10^{-4} mol L^{-1}) in ethanol containing various concentrations of water (total: water + ethanol). Each spectrum was acquired 10 min after Hg^{2+} addition.

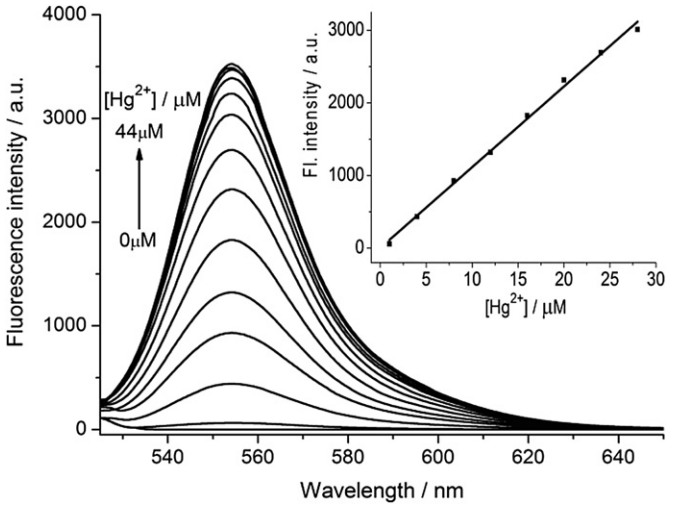

Fig. 13. Fluorescence emission spectra of **L** (2×10^{-5} mol L^{-1}) with addition of various concentrations of $Hg(ClO_4)_2$ in 10% aqueous ethanol solution. Inset: Fluorescence intensity at 552 nm for **L** as a function of the concentration of Hg^{2+} ion. The excitation wavelength is 515 nm.

containing **L** and $Hg(ClO_4)_2$ (Fig. S6). Both peaks disappeared when the medium was switched from organic solvent to aqueous–organic mixtures (v/v, 1:1). Thus, we speculate that the large enhancement of fluorescence intensity in aqueous–organic solution of **L** containing $Hg(ClO_4)_2$ was possibly caused by two-step reaction (Scheme 3b and c). That is Hg^{2+}-promoted ring opening and hydrolysis. In the absence of Hg^{2+}, **L** was colorless and non-fluorescent due to the closed spirolactam ring. The addition of Hg^{2+} ion led to spirocycle opening via coordination. But the **L**–Hg^{2+} complex is just an intermediate compound which would undergo rapid Hg^{2+}-promoted hydrolytic reaction in the presence of water. The second step (Hg^{2+}-promoted hydrolysis) is based on the Hg^{2+}-promoted irreversible hydrolysis of isopropenyl acetate [16] (Scheme 2). We anticipate that a hydrolysis reaction occurs when a similar but modified molecular moiety of isopropenyl acetate was liberated by Hg^{2+}-facilitated ring opening of the spirocycle group (Scheme 3c). However, a new peak at $m/z = 415.4$ (calcd = 415.2) corresponding to rhodamine-19 appeared (Fig. S7) which is solid evidence of the Hg^{2+}-promoted hydrolysis mechanism. Herein, Hg^{2+} acts not only as an analyte but also as the promoter for the hydrolytic reaction.

The fluorescence change that occurs upon addition of water to an ethanol solution containing **L** and Hg^{2+} ion was investigated (Fig. 11). The fluorescence intensity of a solution containing **L** and Hg^{2+} ion declined rapidly with the change of water content from 0% to 10%, and then the fluorescence intensity decreased slowly with the addition of more water (10%–80%). The fluorescence was quenched quickly when the content of water reached 90%. The fluorescence spectrum of a solution of **L** containing Hg^{2+} ion underwent a gradual blue shift with the consecutive addition of water, indicating the reduction of metal-to-ligand charge transfer (MLCT). The blue shift can be explained by the shortened π-electron conjugation system formed by hydrolysis. It is also an evidence of the Hg^{2+}-promoted hydrolysis mechanism. A similar decrease occurs in the UV–Vis absorption of an ethanol solution containing **L** and Hg^{2+} ion with the change of water content in solvents (Fig. 12).

To determine the detection limit, fluorescence titration experiments were performed by mixing various amounts of Hg^{2+} ion with a fixed concentration of **L** in 10% aqueous ethanol solution (Fig. 13). The emission intensity of **L** without metal ions was measured 10 times and the standard deviation of blank measurements was determined. The fluorescence intensity of **L** (2×10^{-5} mol L^{-1}) at 552 nm was found to increase linearly with the concentration of Hg^{2+} in the range of 0.1–2.8 $\times 10^{-5}$ mol L^{-1} ($R^2 = 0.9962$) (Fig. 13, Inset). The detection limit was then calculated with the equation: detection limit $= 3\sigma_{bi}/m$, where σ_{bi} is the standard deviation of blank measurements and m is the slope of the intensity versus sample concentration. The detection limit of Hg^{2+} in 10% aqueous ethanol was measured to be 1.41 $\times 10^{-9}$ mol L^{-1}. According to a Chinese EPA (Environmental Protection Agency) standard, the maximum permissible limit of Hg^{2+} ion in drinking water is 1×10^{-9} kg L^{-1} ($\sim 5.0 \times 10^{-9}$ mol L^{-1}). This means that probe **L** is sensitive enough to monitor the quality of drinking water.

Subsequent experiments using a fluorescence microscope probed the ability of **L** to track Cu^{2+} and Hg^{2+} levels in living cells. To

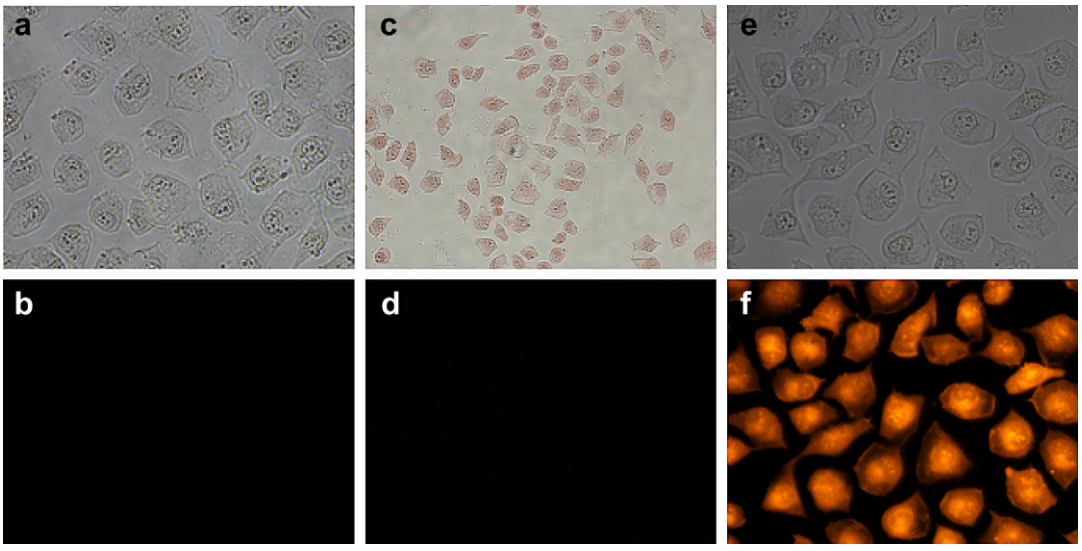

Fig. 14. (TOP) Bright-field transmission images of Human bladder cancer cell line EJ: The EJ cells stained with probe **L** (2.5×10^{-5} mol L^{-1}) for 30 min (a). Image of cells stained with **L** (2.5×10^{-5} mol L^{-1}) and 2.5×10^{-5} mol L^{-1} Cu^{2+} (c) or Hg^{2+} (e) for 30 min (BOTTOM) Fluorescence image of Human bladder cancer cell line EJ: The EJ cells loaded with probe **L** (2.5×10^{-5} mol L^{-1}) for 30 min (b). Fluorescence image cells loaded with **L** (2.5×10^{-5} mol L^{-1}) and 2.5×10^{-5} mol L^{-1} Cu^{2+} (d) or Hg^{2+} (f) for 30 min c and d were obtained under a 20× objective lens, other images were obtained under a 40× objective lens. Incubation was performed at 37 °C.

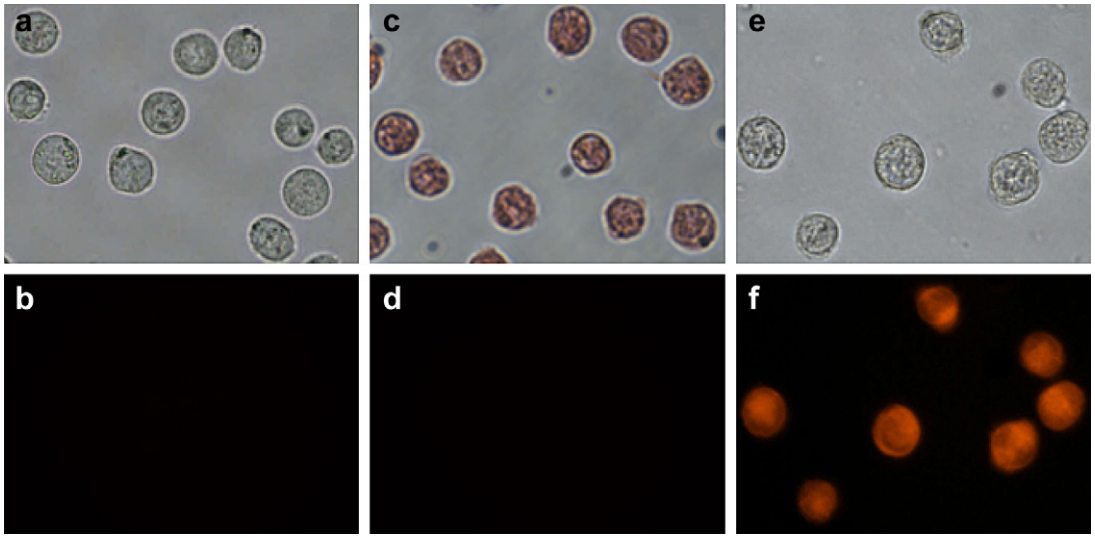

Fig. 15. (TOP) Bright-field transmission images of human leukemia K562 cells: cells loaded with probe **L** (2.5×10^{-5} mol L^{-1}) for 30 min (a). Image of cells supplemented with **L** (2.5×10^{-5} mol L^{-1}) and 2.5×10^{-5} mol L^{-1} Cu^{2+} (c) or Hg^{2+} (e) for 30 min (BOTTOM) Fluorescence image of human leukemia K562 cells: cells loaded with probe **L** (2.5×10^{-5} mol L^{-1}) for 30 min (b). Fluorescence image of cells incubated with **L** (2.5×10^{-5} mol L^{-1}) and 2.5×10^{-5} mol L^{-1} Cu^{2+} (d) or Hg^{2+} (f) for 30 min. All images were obtained under a 40× objective lens. Incubation was performed at 37 °C.

determine the cell permeability of **L**, Human bladder cancer cell line EJ were incubated with **L**. EJ cells incubated with 2.5×10^{-5} mol L^{-1} L for up to 30 min at 37 °C show no intracellular color and no fluorescence. Treatment of EJ cells loaded with 2.5×10^{-5} mol L^{-1} L with Cu^{2+} (2.5×10^{-5} mol L^{-1}) for 30 min at 37 °C, the color changed from colorless to pink (Fig. 14c). But they showed negligible fluorescence. In contrast, incubation of EJ cells stained with 2.5×10^{-5} mol L^{-1} L with Hg^{2+} (2.5×10^{-5} mol L^{-1}) for 30 min at 37 °C displayed remarkably enhanced cytosolic fluorescence (Fig. 14f), and further control experiments without ligand **L** or metal ions gave no fluorescence over background levels. Taken together, theses data clearly demonstrate that the probe is membrane-permeable, and the fluorescence change in the EJ cells was really due to the synchronous appearance of **L** and Cu^{2+} or Hg^{2+}. Thus, probe **L** can be used to image intracellular Cu^{2+} and Hg^{2+} in biological systems. It should therefore be potentially useful in the study of the toxicity or bioactivity of Cu^{2+} and Hg^{2+} in vivo. Fig. 15 displayed the changes in the fluorescence image of **L** stained human leukemia K562 cells after the addition of Cu^{2+} or Hg^{2+} ion. The K562 cells loaded with **L** showed no color and fluorescence. Upon supplementing cells stained with **L** with Cu^{2+} or Hg^{2+}, the K562 cells showed visible pink color and obvious fluorescence (Fig. 15c and f), respectively.

4. Conclusion

In summary, a convenient and highly selective chemosensor **L** based on rhodamine 6G was synthesized and its chemosensing properties were investigated. It can be used as a selective visual chemosensor for Cu^{2+} in natural water, and **L** is also an excellent fluorescence probe for Hg^{2+} based on a proposed Hg^{2+}-promoted hydrolysis mechanism in ethanol–water mixtures. To the best of our knowledge, this is an excellent example of a single molecular sensor capable of detecting multiple metal analytes with different spectral responses. The spectral data and fluorescence image of living cells indicated that **L** could be applied to the detection of Cu^{2+} and Hg^{2+} not only in abiotic systems but also in a biosystem. Thus, **L** can serve as promising chemosensor for Cu^{2+} and Hg^{2+} in environmental monitoring or medical research.

Acknowledgments

This study was supported by the NSFC (Grant Nos. 20771048, 20931003) and the Fundamental Research Funds for the Central Universities (lzujbky-2009-k06). The authors thank Dr. Pamela Holt, Shandong University, for revising the manuscript.

Appendix. Supplementary information

Supplementary information associated with this article can be found, in the online version, at doi:10.1016/j.dyepig.2011.07.010.

References

[1] (a) He Q, Mille EW, Wong AP, Chang CJ. A selective fluorescent sensor for detecting lead in living cells. Journal of the American Chemical Society 2006; 128:9316–7;
(b) de Silva AP, Gunaratne HQN, Gunnlaugsson T, Huxley AJM, McCoy CP, Rademacher JT, et al. Signaling recognition events with fluorescent sensors and switches. Chemical Reviews 1997;97:1515–66.

[2] (a) Muthaup G, Schlicksupp A, Hess L, Beher D, Ruppert T, Masters CL, et al. The amyloid precursor protein of Alzheimer's disease in the reduction of copper(II) to copper(I). Science 1996;271:1406–9;
(b) Løvstad RA. A kinetic study on the distribution of Cu(II)-ions between albumin and transferrin. BioMetals 2004;17:111–3.

[3] (a) Renzoni A, Zino F, Franchi E. Mercury levels along the food chain and risk for exposed populations. Environmental Research 1998;77:68–72;
(b) Boening DW. Ecological effects, transport, and fate of mercury: a general review. Chemosphere 2000;40:1335–51.

[4] (a) Harris HH, Pickering IJ, George GN. The chemical form of mercury in fish. Science 2003;301:1203;
(b) Yoon S, Albers AE, Wong AP, Chang CJ. Screening mercury levels in fish with a selective fluorescent chemosensor. Journal of the American Chemical Society 2005;127:16030–1;
(c) Yoon S, Miller EW, He Q, Do PH, Chang CJ. Angewandte Chemie International Edition 2007;46:6658–61.

[5] (a) Zhang G, Zhang D, Yin S, Yang X, Shuai Z, Zhu D. 1,3-Dithiole-2-thione derivatives featuring an anthracene unit: new selective chemodosimeters for Hg(II) ion. Chemical Communications; 2005:2161–3;
(b) Song KC, Kim JS, Park SM, Chung KC, Ahn S, Chang SK. Fluorogenic Hg^{2+}-selective chemodosimeter derived from 8-hydroxyquinoline. Organic Letters 2006;8:3413–6;
(c) Sancenón F, Martínez-Máñez R, Soto J. 1,3,5-Triarylpent-2-en-1,5-diones for the colorimetric sensing of the mercuric cation. Chemical Communications 2001;21:2262–3;
(d) Gunnlaugsson T, Leonard JP, Murray NS. Highly selective colorimetric naked-eye Cu(II) detection using an azobenzene chemosensor. Organic Letters 2004;6:1557–60;

(e) Youn NJ, Chang SK. Dimethylcyclam based fluoroionophore having Hg^{2+}- and Cd^{2+}-selective signaling behaviors. Tetrahedron Letters 2005;46:125–9;
(f) Xiang Y, Tong AJ, Jin PY, Ju Y. New fluorescent rhodamine hydrazone chemosensor for Cu(II) with high selectivity and sensitivity. Organic Letters 2006;8:2863–6;
(g) Wu JS, Hwang IC, Kim KS, Kim JS. Rhodamine-based Hg-selective chemodosimeter in aqueous solution: fluorescent OFF-ON. Organic Letters 2007; 9:907–10;
(h) Yuan MJ, Zhou WD, Liu XF, Zhu M, Li JB, Yin XD, et al. A multianalyte chemosensor on a single molecule: promising structure for an integrated logic gate. The Journal of Organic Chemistry 2008;73:5008–14;
(i) Lee MH, Kim HJ, Yoon S, Park N, Kim JS. Metal ion induced FRET OFF-ON in tren/dansyl-appended rhodamine. Organic Letters 2008;10:213–6;
(j) Suresh M, Shrivastav A, Mishra S, Suresh E, Das A. A rhodamine-based chemosensor that works in the biological system. Organic Letters 2008;10:3013–6;
(k) Chereddy NR, Thennarasu S. Synthesis of a highly selective bis-rhodamine chemosensor for naked-eye detection of Cu^{2+} ions and its application in bioimaging. Dyes and Pigments 2011;91:378–82;
(l) Peng XH, Wang YJ, Tang XL, Liu WS. Functionalized magnetic core-shell Fe_3O_4@SiO_2 nanoparticles as selectivity-enhanced chemosensor for Hg(II). Dyes and Pigments 2011;91:26–32;
(m) Wang HH, Xue L, Yu CL, Qian YY, Jiang H. Rhodamine-based fluorescent sensor for mercury in buffer solution and living cells. Dyes and Pigments 2011;91:350–5.

[6] (a) Zhu M, Yuan M, Liu X, Xu J, Lv J, Huang C, et al. Visible near-infrared chemosensor for mercury ion. Organic Letters 2008;10:1481–4;
(b) Coskun A, Yilmaz MD, Akkaya EU. Bis(2-pyridyl)-substituted boratriazaindacene as an NIR-emitting chemosensor for Hg(II). Organic Letters 2007;9:607–9;
(c) Avirah RR, Jyothish K, Ramaiah D. Dual-mode semisquaraine-based sensor for selective detection of Hg^{2+} in a micellar medium. Organic Letters 2007;9:121–4;
(d) Zhang X, Shiraishi Y, Hirai T. Cu(II)-selective green fluorescence of a rhodamine–diacetic acid conjugate. Organic Letters 2007;9:5039–42.

[7] (a) Kwon JM, Jang YJ, Lee YJ, Kim KM, Seo MS, Nam W, et al. A highly selective fluorescent chemosensor for Pb^{2+}. Journal of the American Chemical Society 2005;127:10107–11;
(b) Lee MH, Wu JS, Lee JW, Jung JH, Kim JS. Highly sensitive and selective chemosensor for Hg^{2+} based on the rhodamine fluorophore. Organic Letters 2007;9:2501–4;
(c) Ko SK, Yang YK, Tae J, Shin I. In vivo monitoring of mercury ions using a rhodamine-based molecular probe. Journal of the American Chemical Society 2006;128:14150–5.

[8] Lakowicz JR. Principles of fluorescence spectroscopy. 3rd ed. New York: Springer; 2006.

[9] Mao J, Wang LN, Dou W, Tang XL, Yan Y, Liu WS. Tuning the selectivity of two chemosensors to Fe(III) and Cr(III). Organic Letters 2007;9:4567–70.

[10] (a) Komatsu H, Miki T, Citterio D, Kubota T, Shindo Y, Kitamura Y, et al. Single molecular multianalyte (Ca^{2+}, Mg^{2+}) fluorescent probe and applications to bioimaging. Journal of the American Chemical Society 2005;127:10798–9;
(b) Caballero A, Espinosa A, Tárraga A, Molina P. Ferrocene-based small molecules for dual-channel sensing of heavy- and transition-metal cations. The Journal of Organic Chemistry 2008;73:5489–97.

[11] de Mello JC, Wittmann HF, Friend RH. An improved experimental determination of external photoluminescence quantum efficiency. Advanced Materials 1997;9:230–2.

[12] Wu D, Huang W, Duan CY, Lin ZH, Meng QJ. Highly sensitive fluorescent probe for selective detection of Hg^{2+} in DMF aqueous media. Inorganic Chemistry 2007;46:1538–40.

[13] Anthoni U, Christophersen C, Nielsen P, Puschl A, Schaumburg K. Structure of red and orange fluorescein. Structural Chemistry 1995;3:161–5.

[14] Vosburgh WC, Copper GR. Complex ions. I. The identification of complex ions in solution by spectrophotometric measurements. Journal of the American Chemical Society 1941;63:437–42.

[15] Kim JS, Quang DT. Calixarene-derived fluorescent probes. Chemical Reviews 2007;107:3780–99.

[16] (a) Du J, Fan J, Peng X, Sun P, Wang J, Li H, et al. A new fluorescent chemodosimeter for Hg^{2+}: selectivity, sensitivity, and resistance to Cys and GSH. Organic Letters 2010;12:476–9;
(b) Abley P, Byrd JE, Halpern J. Mercury(II)- and thallium(III)-catalyzed hydrolysis of isopropenyl acetate. Journal of the American Chemical Society 1972;94:1985–9.